Centrifugal Analysis of Pivoted-Rotor Systems for Capillary Pressure Measurements

Z. Andy Chen and Douglas W. Ruth
Dept. of Mechanical and Industrial Engineering, University of Manitoba, Winnipeg, Man., Canada R3T 5V6

The fundamental theory on centrifuge determination for capillary pressures was laid by Hassler and Brunner in 1945. Christiansen (1992) and Ayappa et al. (1994) demonstrated the significance of the *radial effect*. Forbes et al. (1994) reexamined quantitatively the radial effect by using a simplified analytical solution to the double-integral model. More recently Chen and Ruth (1995) developed a three-dimensional model characterizing the whole centrifugation mechanism. They found that gravitational acceleration also plays an important role and is most pronounced at speeds $\omega < 500$ rpm, and that this effect leads to inaccurate interpretations of capillary pressure information at high saturation, near the threshold pressure. A remedial approach by means of numerical parameter estimation techniques was discussed recently (Chen and Ruth, 1994), and an experimental attempt by redesigning a pivoted rotor configuration was reported by Pohjoisrinne et al. (1996). This note outlines the result of a theoretical investigation of the pivoting rotor physics to support the experimental study.

Conventional Beckman centrifuges have fixed, horizontal rotors, stretching out from the central axis of rotation. Such a configuration is depicted in Figure 1. The basic equation for describing the centrifugation process is given by

$$P_c = \frac{1}{2}\Delta\rho\omega^2(x^2 + y^2) - \Delta\rho g z + C. \tag{1}$$

Defining $C_g = 2g/\omega^2$, which characterizes the inclination of the true acceleration field distribution in the equipotential surface, capillary pressure at any point inside the core plug is

$$P_c(r, z) = \frac{1}{2}\Delta\rho\omega^2\left(r_{0\max}^2 - r^2 - C_g(R - z)\right), \tag{2}$$

where $r_{0\max}$ is the maximum reference rotation radius, and the capillary pressure for this reference radius, which is the maximum-capillary pressure in the sample, is

$$P_c = \frac{1}{2}\Delta\rho\omega^2(r_{0\max}^2 - r_{0\min}^2). \tag{3}$$

Zero-capillary pressure occurs at the two tangent points that are defined by the intersection of the paraboloid of revolution characterized by $r_{0\max}$ and the edge of the outside endface. Details on the horizontal rotor investigation were reported elsewhere (Chen and Ruth, 1995).

Pivoted-Rotor Systems

The idea of adopting a pivoted-rotor head was conceived to overcome the difficulties of fixed, horizontal rotor centrifuges. It is logically postulated that if the gravity and gravitational acceleration fields at a right angle in the fixed-rotor head create a downward dragging effect, then a tilted rotor configuration can make the gravitational and centrifugal acceleration fields more closely aligned, thereby minimizing this effect. Even though this method has been used in practice (Forbes and Fleury, 1994), no theoretical foundation has ever been laid to support the practice.

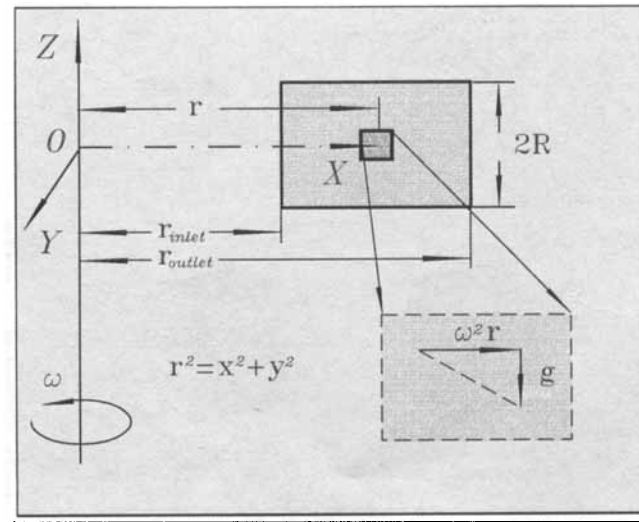

Figure 1. Gravity degradation effect.

Current address of Z. A. Chen: Schlumberger of Canada, 801-6th Avenue, S.W., Calgary, Alta., Canada T2P 3W2.

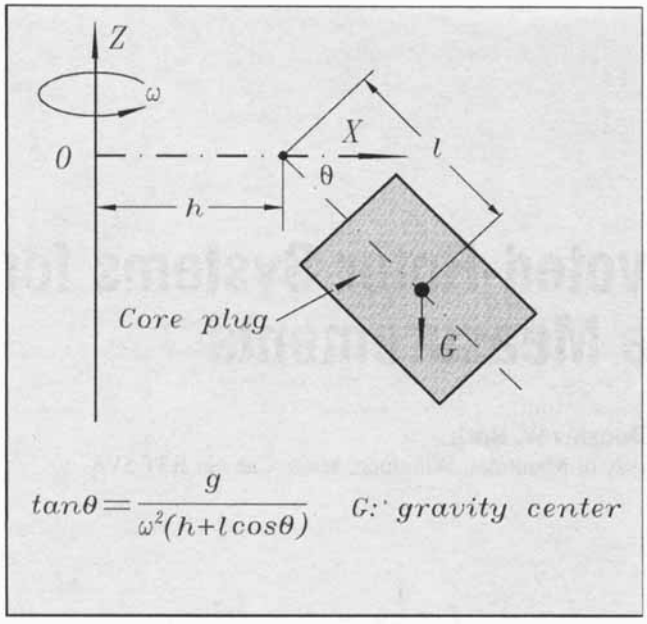

Figure 2. Pivoted rotor centrifuge configuration.

Figure 2 shows a general configuration for a pivoted rotor system that can be extended to several practical scenarios. The inclination angle θ of the core plug for the general case is determined by

$$\tan\theta\left(1+\frac{l}{h}\cos\theta\right)=\frac{g}{\omega^2 h}. \tag{4}$$

Iterations are required to determine the inclined angle θ vs. the spinning speeds for the general cases (Figure 3). Only small changes in the value of θ result from changes in the values of h and l.

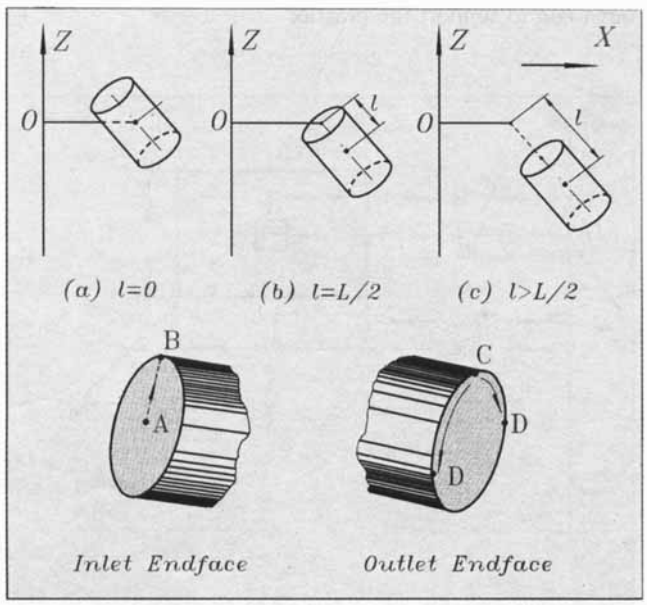

Figure 3. Various hookup scenarios.

Boundary Capillary Pressures

In order to calculate the capillary pressure distribution, boundary capillary pressures have to be determined. In a horizontal rotor head, the maximum-capillary pressure during the experiment occurs at the top right edge of the inlet endface of the core, which is a fixed point. Furthermore, zero-capillary pressure occurs at the outlet endface, but the location of this zero-capillary pressure is not a fixed point; it occurs at two points sliding along the outside perimeter edges of the lower portion of the endface.

For the pivoted-rotor system, the locations for the maximum- and zero-capillary pressures are again in the two endfaces. There are various configurations for the pivoted systems, depending on how the rotor bucket is hooked up, and where the center of gravity of the bucket/core system is located. In setting up a practical configuration, it must be stressed that the core plug should be installed such that the center of gravity of the core plug (the fluids in the plug form an independent inclined system) is also the center of gravity of the whole combined rotor system—the system including both the core plus the bucket. This installation is required in order to ensure that the centrifugal field distribution in the core plug conforms with the inclination of the whole rotor system. If not, it would be very difficult to consider the centrifugal field of the inclined core plug, in addition to a separate inclination of the whole rotor system.

One way to understand the changes of the capillary boundary pressures is to do numerical searches at the two endfaces of the core plug during a simulated experiment. Equation 1 is sufficient to calculate the capillary pressures at the two endfaces for all points in these areas. Numerical tests have been run for various configurations with pivoted rotor systems. The numerical search for the maximum-capillary pressure point is carried out with Eq. 1, assuming the constant C is zero in the equation and calculating pressure values in the whole endface area. The maximum pressure point in the area, which corresponds to the maximum-capillary pressure point, can then be determined. It has been found that the maximum-capillary pressure takes place at the central line of the inlet endface of the core plug, and also that it changes as rotational speeds increase. When we look at the track of the maximum-capillary pressure on the inlet endface of the core plug as θ changes from $\pi/2$ to zero, corresponding to the transition state from the motionless to the fixed, horizontal rotor case, it has been found that the point $\boldsymbol{A}$ for the motionless state gives the maximum-capillary pressure. Relative to the core plug itself, this point moves from $\boldsymbol{A}$, the central point, to $\boldsymbol{B}$, the right top edge point of the inlet endface area as θ changes from $\pi/2$ to zero (Figure 3). Therefore, the reference point for the maximum-capillary pressure varies. The range of the moving track of the maximum-capillary pressure at the inlet is equal to the radius of the core plug. Following a similar scheme, searching for the maximum-capillary pressure point, the zero-capillary pressure has also been found. It occurs at the upper edge of the outlet endface perimeter: two points sliding from $\boldsymbol{C}$ to $\boldsymbol{D}$ when the inclination angle θ changes from $\pi/2$ to zero.

Compared with the case of the fixed-rotor system, the boundary conditions for both the maximum- and zero-capillary pressures become more complicated. The exact location of both the maximum- and zero-capillary pressure

boundary conditions can be numerically calculated as $(x, y, z) \Rightarrow \theta(\omega)$, and numerical calculations can exactly define the location of this point vs. the inclination angle. Numerical experiments for configurations with various combinations of h and l show that at the speeds when the maximum capillary pressure point is moving from A to B, the zero-capillary pressure point stays at the top right edge point. Once the maximum pressure has reached B, the zero-capillary pressure points begin to move down along the two edges of the outlet endface of the core plug. This trend held for all hookup configurations investigated.

Analytical Approach

The preceding numerical observations can also be supported by analytical derivations. If we look at the geometry of a pivoted core plug in Case (c) in Figure 3, the maximum-and zero-capillary pressure points are determined by the locations where the paraboloid of revolution just "touches" the *inclined* round planes of the two endfaces of the core plug. The "touching" point at the inlet endface corresponds to the maximum-capillary pressure point, which turns out to be a point sliding from A to B. At the outlet endface, it corresponds to the zero-capillary pressure point, which includes two points moving down along the edge of the endface from C to D.

The mathematical description of the two endface planes is given by

$$\begin{cases} y^2 + [(x-h)\sin\theta + z\cos\theta]^2 = R^2 \\ (x-h)\cos\theta - z\sin\theta \in \left(l - \dfrac{L}{2}, l + \dfrac{L}{2}\right). \end{cases} \tag{5}$$

When we look at the inlet endface for the maximum-capillary pressure condition, where $y = 0$, a straight line characterizing the track of $A \Rightarrow B$ can be defined. From the preceding equation, we can write the round plane equation at $y = 0$ as (the second expression of Eq. 5 for the inlet endface)

$$z = \frac{(x-h)\cos\theta - \left(l - \dfrac{L}{2}\right)}{\sin\theta}. \tag{6}$$

This expression is substituted into the differential capillary pressure equation derived from Eq. 1 for the case of $y = 0$. The result is

$$\frac{dP_c}{dx} = \Delta\rho\left(\omega^2 x - \frac{g}{\tan\theta}\right). \tag{7}$$

The extremum for P_c is given by the condition $(dP_c/dx) = 0$. Applying this condition to Eq. 4 and combining the result with Eq. 7, will lead to

$$x^0 = \frac{g}{\omega^2 \tan\theta} = h + l\cos\theta. \tag{8}$$

This equation gives the x-coordinate of the track of A to B for a given speed. Accordingly,

$$y^0 = 0 \tag{9}$$

and

$$z^0 = \frac{L}{2}\frac{1}{\sin\theta} - l\sin\theta. \tag{10}$$

As the rotational speed increases, the outside surface of the mathematical object of the paraboloid tends to become steeper, while the inlet endface plane of the core plug is swung outward, being bounded by the circle edge. The mathematically defined point of the extremum eventually moves outside the endface plane. Once this occurs, the extremum inside the endface is fixed at B.

If we look at the local distance of the moving maximum-capillary pressure track (obviously it is within [0, R]), and using Eq. 4, we get

$$R\cos\omega = \frac{x^0 - [h + (l - L/2)\cos\theta]}{\tan\theta}. \tag{11}$$

Equations 8 and 11 will result in

$$\tan\theta_{crit1} = \frac{L}{2R}. \tag{12}$$

In this equation, θ_{crit1} is determined by the configuration of the pivoted system (Eq. 4) and gives the angle that coincides with the arrival of the maximum-capillary pressure point at B. When the core diameter is equal to the core length $L = 2R$, the angle is $\pi/4$, regardless of the combination of the hookup parameters. For a core plug sample, when $r = R$, this angle θ_{crit1} reaches its peak bounded by the inlet endface, and in particular for the inlet endface, when the rotational speed is such that the inclination angle θ is a 45°, the maximum capillary pressure point arrives at B. The critical speed is thus determined according to Eq. 4 by

$$\omega_{crit1} = \sqrt{\frac{g}{\tan\theta_{crit1}(h + l\cos\theta_{crit1})}}. \tag{13}$$

After this critical speed, the maximum-capillary pressure stays at the point at the top right edge of the inlet endface. For the maximum-capillary pressure point, its moving track is defined by two sets of solutions. When $\pi/2 \geq \theta_{crit1} \geq \tan^{-1}(L/2R)$, the track of the moving point is determined by

$$\begin{cases} x^0 = h + l\cos\theta \\ y^0 = 0 \\ z^0 = \dfrac{L}{2}\dfrac{1}{\sin\theta} - l\sin\theta, \end{cases} \tag{14}$$

while when $\tan^{-1}(L/2R) \geq \theta_{crit1} \geq 0$, the track is determined by

$$\begin{cases} x^0 = h + R\sin\theta + \left(l - \dfrac{L}{2}\right)\cos\theta \\ y^0 = 0 \\ z^0 = R\cos\theta - \left(i - \dfrac{L}{2}\right)\sin\theta. \end{cases} \tag{15}$$

Similarly at the outlet endface, we obtain the following expressions:

$$x_0 = h + l\cos\theta + \frac{L}{2}\frac{1}{\cos\theta} \tag{16}$$

$$y_0 = \pm\sqrt{R^2 - \left(\frac{L}{2}\tan\theta\right)^2} \tag{17}$$

and

$$z_0 = -l\sin\theta. \tag{18}$$

As for the maximum-capillary pressure case, conditions will have to be imposed on these solutions. In order to make the y_0 meaningful, the following condition must apply

$$R^2 - \left(\frac{L}{2}\tan\theta\right)^2 \geq 0. \tag{19}$$

This leads to

$$\tan\theta_{\text{crit2}} \leq \frac{2R}{L}. \tag{20}$$

This tells us that only after the speed reaches a value such that the tangent of the inclination angle is given by Eq. 20, will the zero-capillary pressure point start to slide down along the two edges of the circular outlet endface, regardless of the hookup configuration of the rotor system. Below this speed, the zero-capillary pressure point stays at the point at the top edge of the outlet endface. Therefore, two sets of equations are found to determine the zero-capillary pressure condition. When $\tan^{-1}(2R/L) \geq \theta_{crit2} \geq 0$, we have

$$\begin{cases} x_0 = h + l\cos\theta + \dfrac{L}{2}\dfrac{1}{\cos\theta} \\ y_0 = \pm\sqrt{R^2 - \left(\dfrac{L}{2}\tan\theta\right)^2} \\ z_0 = -l\sin\theta, \end{cases} \tag{21}$$

and when $\pi/2 \geq \theta_{crit2} \geq \tan^{-1}(2R/L)$, we have

$$\begin{cases} x_0 = h + R\sin\theta + \left(l + \dfrac{L}{2}\right)\cos\theta \\ y_0 = 0 \\ z_0 = R\cos\theta - \left(l + \dfrac{L}{2}\right)\sin\theta. \end{cases} \tag{22}$$

The preceding equations match the results from the numerical search calculations.

It can be concluded that the core geometry plays an important role in the distribution of the centrifugal field inside the core plug. When a plug is cut such that $L = 2R$, 45° is a critical angle for the boundary-capillary pressure values at both the inlet and the endlet endfaces. If $L > 2R$, a slender core plug, the zero-capillary pressure points will begin to move down even before the maximum-capillary pressure point arrives at B while if $L < 2R$, indicating a chunky core plug, the maximum-capillary pressure point will arrive at the top edge of the inlet endface before the zero-capillary pressure points start to slide down. These results are important in the design of a pivotal system.

Capillary Pressure Calculation

In order to calculate the capillary pressure distribution inside the core plug, we have to use the zero-capillary pressure conditions. Equation 1 gives the capillary pressure at any point inside the core plug:

$$P_c = \frac{1}{2}\Delta\rho_{w-nw}\omega^2\left(x^2 + y^2 - C_g z\right) + C. \tag{23}$$

Substituting the numerically calculated zero-capillary pressure boundary condition will lead to the general equation for capillary pressure calculations

$$P_c = \frac{1}{2}\Delta\rho_{w-nw}\omega^2\left(C_0 - x^2 - y^2 + C_g z\right), \tag{24}$$

where the constant $C_0 = x_0^2 + y_0^2 - C_g z_0$, and x_0, y_0, and z_0 take the values of the zero-capillary pressure point based on Eqs. 21 and 22, as a function of the inclination angle θ that will be determined for the rotational speed ω according to Eq. 4. Similarly, the maximum-capillary pressure for reference is

$$P_c = \frac{1}{2}\Delta\rho_{w-nw}\omega^2\left(C_0 - (x^{02}) - (y^{02}) + C_g z^0\right), \tag{25}$$

where the x^0, y^0, z^0 are calculated from Eqs. 14 and 15, the maximum-capillary pressure values, as functions of the inclination angle θ. Following a procedure similar to that used in the fixed-rotor analysis, a mean saturation balance equation can be defined for saturation conversion purposes.

Centrifugal Field Distributions

It has been demonstrated that the inclination of the centrifugal field due to the vertical gravitational acceleration causes trouble for capillary pressure calculations at low initial rotation speeds $\omega < 500$ rpm. The extent to which the centrifugal field inclines can be illustrated by the slope of the inclined equipotential surfaces inside the core plug. From Eq. 1 we can get $dP_c = 0$ for an equipotential surface; therefore, this surface is described by the equation

$$\frac{dx}{dz} = \frac{g}{\omega^2}\frac{1}{x} = \frac{C_g}{2x}. \tag{26}$$

Consider a typical centrifuge rotor with a one-inch-long and one-inch-diameter core sample. The related geometrical parameters include: $r_{inlet} = 6.06$ cm, $r_{outlet} = 8.6$ cm, and $R = 1.27$ cm. A calculation was made to find the slope dx/dz at the inlet endface $x = r_{inlet} = 6.06$ cm. At lower speeds, this slope varies dramatically due to the changes of C_g. When the angular speed takes values of $\omega = 10$, 20, 30, 40, and 50 rpm, dx/dz at the inlet endface $x = r_{inlet}$ is 147.6, 36.9, 16.4, 9.2, and 5.9, respectively.

A transformation of Cartesian coordinates will be made from the X-Y-Z system into the X'-Y'-Z' system, where the prime denotes the coordinate for the pivoted-rotor system, and the origin of the X'-Y'-Z' coordinate system is located at the center of gravity of the pivoted-rotor head as defined in Figure 2. For the pivoted cases, equations describing an equivalent slope of dx'/dz' can be derived. For Case (a) in Figure 3, we use $x = h + x'\cos\theta + z'\sin\theta$, $y = y'$, and $z = -x'\sin\theta + z'\cos\theta$ to conduct the coordinate transformation. The resulting expression for the slope in a pivoted core plug is

$$\frac{dx'}{dz'} = -\frac{\cos\theta\sin\theta(x'\cos\theta + z'\sin\theta)}{h + \cos^2\theta(x'\cos\theta + z'\sin\theta)}. \tag{27}$$

For the same seven rotation speeds, with $h = 7.33$ cm, and $l = 0.00$ cm, the slopes dx'/dz' become 0.0001, 0.0002, 0.0009, 0.0029, and 0.0069, respectively, at the same speeds. These values of h and l were chosen so that when the rotation speed is such that the core plug is spinning almost horizontally, the system looks identical to the fixed-rotor case. This is done to make comparisons simpler.

A numerical search of Eq. 27 has been conducted to study the general trend of slope changes. It has been found through this search that the maximum slope dx'/dz' for this case is 0.1341 and occurs at the bottom right edge of the inlet endface of the core plug when $\theta = 45°$. However, the slope generally varies very little, with a mean value of 0.0264 across the whole core sample. The slope at the inlet endface of the core plug, where the maximum slope occurs, also does not vary much, with a mean value of 0.03989. Even with $\theta = 45°$, which we suspect causes the biggest slope change, the mean value is about 0.0446, still much less than the slope when $\omega = 500$ rpm for the fixed-rotor system. Therefore, the distortion of the equipotential surfaces inside the core plug can be greatly minimized if a pivoted rotor head is used.

Similarly, a transformation is performed for the general situation—Case (c) in Figure 3—leading to a similar equation for the calculation of the slope. For this general case, $x = h + x'\cos\theta + (l + z')\sin\theta$, $y = y'$, and $z = -x'\sin\theta + (l + z')\cos\theta$ are used to do the transformation, which leads to the slope equation ($l = 0$ will recover Eq. 27)

$$\frac{dx'}{dz'} = \frac{\frac{C_g}{2}\cos\theta - \sin\theta[h + x'\cos\theta + (l + z')\sin\theta]}{\frac{C_g}{2}\sin\theta + \cos\theta[h + x'\cos\theta + (l + z')\sin\theta]}. \tag{28}$$

Taking $h = 6.06$ cm, $l = 1.27$ cm, and $h = 4.79$ cm, $l = 2.54$ cm, respectively (both cases will almost be reduced to the fixed horizontal system when the spinning rate goes over 500 rpm), the slope changes are plotted in Figure 4. It can be seen that the slopes of the distorted equipotential surfaces have been much reduced. Also plotted in this figure are the results for the case $h = 10.0$ cm and $l = 3.0$ cm. This case shows the least slope change, suggesting that *the longer the arm the better.*

Ideally, we would hope to completely eliminate distortions of the surfaces, corresponding to a zero slope ($dx'/dz' = 0$). This is impossible to do, however, unless there is no gravity acceleration ($g = 0$ gives $\theta = 0$, and thus $dx'/dz' = 0$). When $\theta = 0$ and $\pi/2$, we are indeed able to get $dx'/dz' = 0$ in the pivoted-rotor head and keep the slope changes at a very low level, while for the horizontal head, the slope becomes extremely large for low speeds (large inclination angles) and approaches infinite when θ approaches $\pi/2$. Therefore, the pivoted rotor is much superior to the fixed rotor in minimizing the gravity degradation effect, making the true centrifugal field inside the core plug more like the traditionally assumed conditions under which standard data-interpretation techniques were established. Under such circumstances, curvature of the surfaces for isopotentials is due to the radial effect, a two-dimensional geometrical concern. Figure 5 demonstrates the true scenario of an equipotential surface for a pivoted core plug at low speeds. Three low speeds, 110 rpm, 200 rpm, and 400 rpm, were used, helping us to visualize the variation of the surface (Figures 5a, 5b, and 5c).

In order to illustrate the equipotential contours inside the core plug, we redepicted such contours with given geometrical parameters. An equation characterizing isopotential contours inside the titled core plug was obtained as

$$x' = -\frac{1}{\cos^2\theta}\left(\frac{h}{\cos\theta} + \frac{z'\sin 2\theta}{2}\right) + \frac{\sqrt{\left(\frac{h}{\cos\theta} + \frac{z'\sin 2\theta}{2}\right)^2 - \cos^2\theta(z'^2\sin^2\theta + y'^2 + h^2 - r_0^2 + 2hR\tan\theta)}}{\cos^2\theta} \tag{29}$$

This equation is valid for Case (a) in Figure 3, where h is taken as $(r_{inlet} + r_{outlet})/2$ and $l = 0$. The equipotential surface in Figure 6 is drawn for the inclination angle of 45°, because this causes the maximum slope according to the previous calculations. Other angles from 0 to $\pi/2$ can also be drawn, as in Figure 7, which gives a surface at 200 rpm corresponding to 17° under the given condition. These equipotential surfaces do not show any serious distortions such as those observed for the fixed-rotor system. Therefore, it is observed

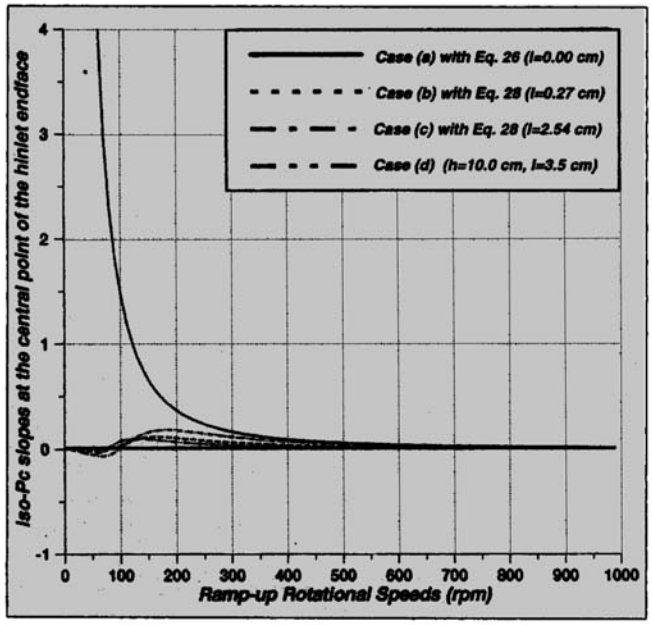

Figure 4. Comparison of slopes during ramp-ups.

that even if the inclination angle is relatively large at low speed, the equipotential contour is much different from that for the fixed-rotor system, and the new contour (the pivoted model) is basically similar to the no-gravity, horizontal case. Figure 8 shows the equipotential surface drawn in the real centrifugation coordinate system with the same geometrical inputs as those in Figure 7; what occurs is a much distorted surface inside the core plug. Therefore, even though we cannot completely eliminate the deformation of the equipotential surface, the deformation has become much less serious in a pivoted system. The centrifugal field distribution can be reasonably or at least approximately assumed to simulate the conditions under which all current data-interpretation algorithms are valid.

Closed-form equations for describing the isopotential contours for Cases b and c in Figure 3, would be extremely difficult to derive. Since we have shown that almost the same slope distributions occur for these cases, we can thus conclude that Figure 6 represents the general pivoted case in comparison with the fixed horizontal case.

Reference Capillary Pressures

A comparison of the maximum-reference-capillary pressures for the fixed and the pivoted systems has been made using Eqs. 3 and 25. Synthesized centrifuge experimental data sets were used. Figure 9 shows the result of this comparison. The rotation speed ranges from extremely low (10 rpm) to 1,000 rpm. Three typical rotor geometrical parameter sets are adopted: the first one has a rotor arm of $h = 7.33$ cm and a tilting arm of $l = 0.00$ cm; the second one has a $h = 6.06$ cm rotor arm of, and a tilting arm of $l = 1.27$ cm; the third one has a rotor arm of $h = 4.79$ cm and a tilting arm of $l = 2.54$ cm. Core sample sizes are all 2.54 cm in diameter and 2.54 cm in length. These three configurations represent the three typical designs in Figure 3. P_{ch} denotes the maximum-reference-capillary pressure for the fixed-rotor system (obtained from Eq. 3), and P_{cv} denotes the maximum-reference-capillary pressures, calculated according to Eq. 25.

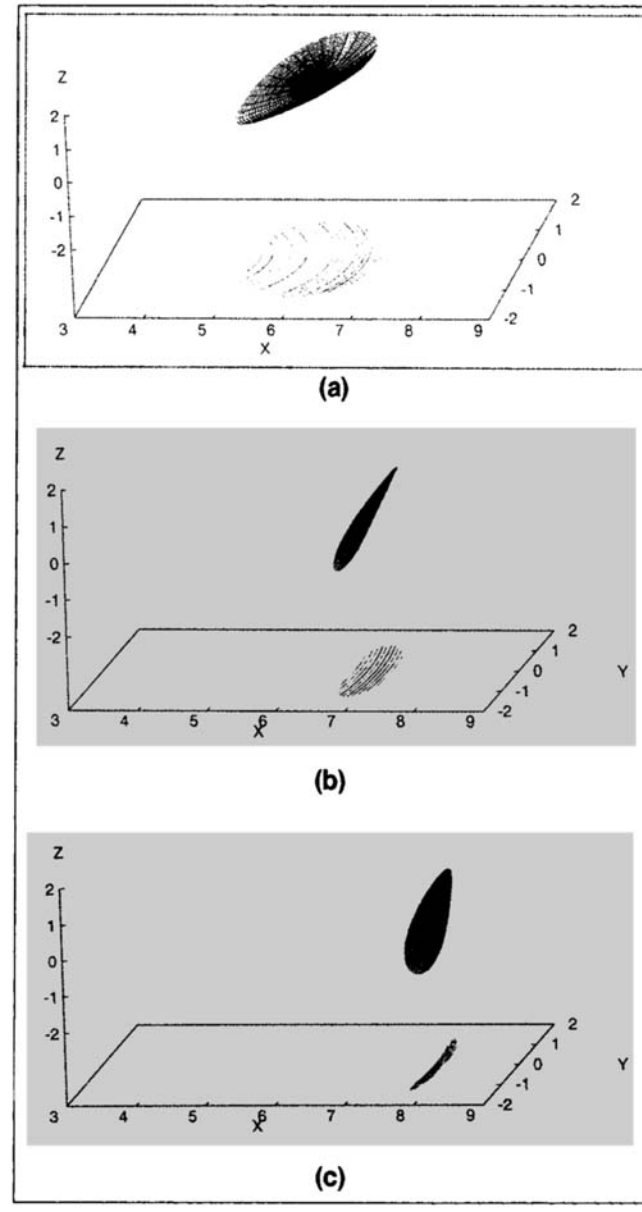

Figure 5. Visualization of an equipotential surface for pivoted cases: (a) 110 rpm; (b) 200 rpm; (c) 400 rpm.

From Figure 9 we can see that the ratios become unity with elevated angular speeds when the speed exceeds 500 rpm, indicating that the gravity effect vanishes. In the low-speed range from 10 rpm to 500 rpm, the ratios decrease and arrive at a maximum when the speed is around 100 rpm. This phenomenon is caused by the fact that both the maximum and the zero-reference-capillary pressures for the pivoted-rotor system have dramatic changes compared with the fixed-rotor head. At speeds below 200 rpm, data analysis would be very complex. The parameter estimation technique appears to be the only possible method.

Further comparisons were also made regarding the geometrical parameters of a core plug, to study the impact of L and R on the capillary pressure distribution fields. Slender and chunky core plugs are reflected in these two parameters. Typical parameters were assigned to the length and radius of

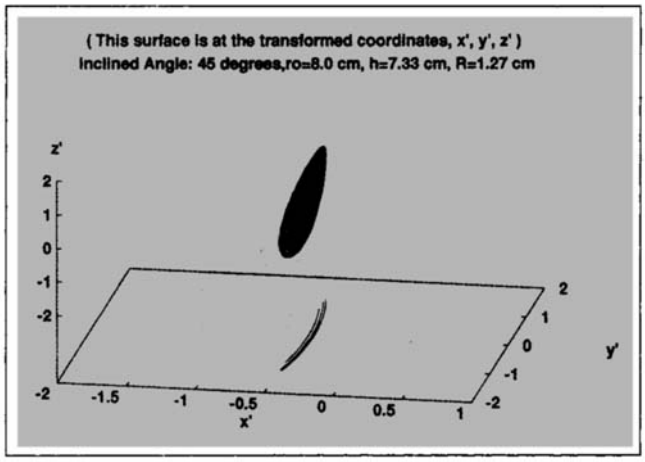

Figure 6. 3-D model: gravity effect minimized for pivoted case of 45° inclination.

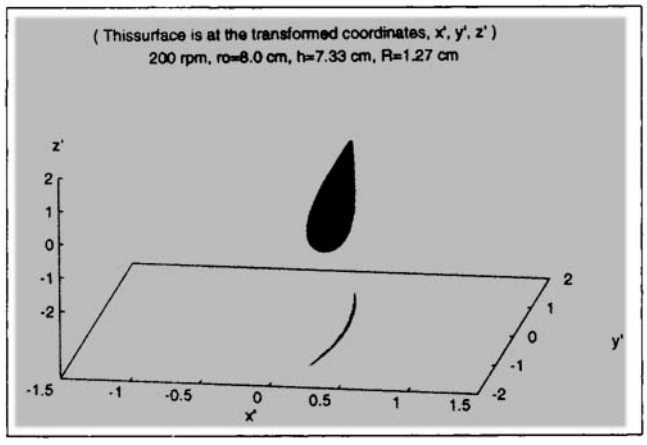

Figure 7. 3-D model: gravity effect minimized for pivoted case of 200 rpm in local coordinate.

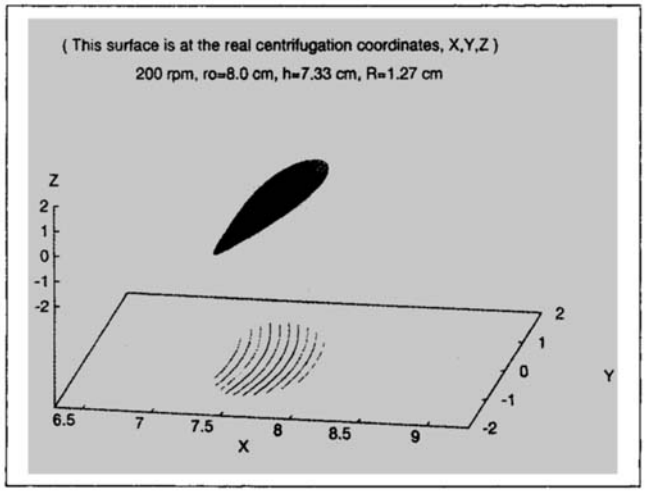

Figure 8. 3-D model: gravity effect minimized for pivoted case of 200 rpm in real coordinate.

a core plug, and it was observed that long slim core plugs using a pivoted system provide more closely centrifugal fields to the fixed-rotor system, than short chunky core plugs. For

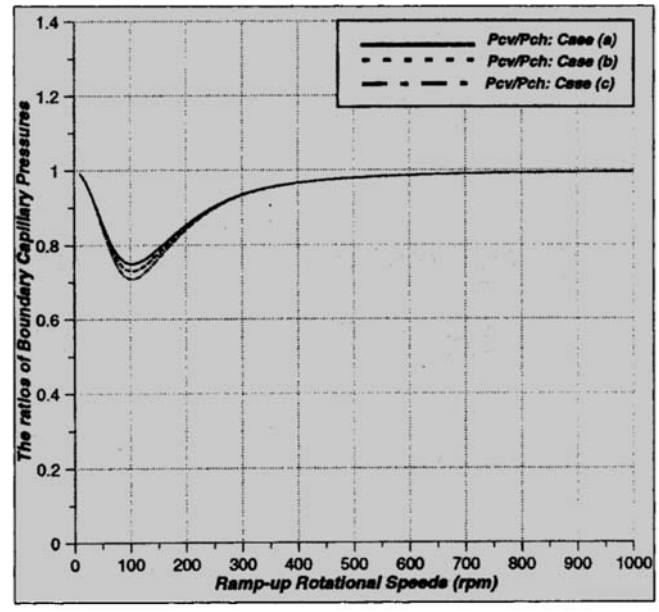

Figure 9. Ratios of boundary capillary pressures during ramp-ups.

all cases, data sets under 200 rpm will be much less practical for interpretation.

Notation

C_0 = constant
C_g = characteristic factor
h = horizontal rotation length
l = pivoting arm length
L = length of core plug
R = radius of core plug
r = rotation radius
r_{inlet} = horizontal distance of core plug inlet
r_{outlet} = horizontal distance of core plug outlet
$r_{0\,min}$ = minimum reference rotation radius
α = characteristic angle
$\Delta\rho$ = density difference of fluid pairs
ω = angular rotation speed

Literature Cited

Ayappa, K. G., E. A. Abraham, H. T. Davis, E. A. Davis, and J. Gordon, "Influence of Sample Width on Deducing Capillary Pressure Curves with the Centrifuge," *Chem. Eng. Sci.*, **49**, 327 (1994).

Chen, Z. A., and D. W. Ruth, "Centrifuge Capillary Pressure Data Interpretation: Gravity Degradation Aspect Consideration," *SCA Int. Symp.*, Stavanger, Norway (1994).

Chen, Z. A., and D. W. Ruth, "The Effect of Gravity Degradation on Low-Speed Centrifuge Capillary Pressure Data," *AIChE J.*, **41**(3), 469 (1995).

Christiansen, R. L., "Geometric Concerns for Accurate Measurement of Capillary Pressure Relationships with Centrifuge Methods," *SPE Form. Eval.*, **7**, 311 (1992).

Forbes, P. L., Z. A. Chen, and D. W. Ruth, "Quantitative Analysis of Radial Effects on Centrifuge Capillary Pressure Curves," SPE Tech. Conf. and Exhibition, New Orleans, LA (1994).

Forbes, P. L., and M. Fleury, Institut Français du Pétrole, private communications (1994).

Hassler, G. L., and E. Brunner, "Measurement of Capillary Pressures in Small Samples," *Trans. AIME*, **160**, 114 (1945).

Pohjoisrinne, T., D. W. Ruth, and Z. A. Chen, "A Capacitance Based Measurement System for Produced Fluids in a Pivoted or Horizontal Centrifuge," Int. Symp. of the SCA Int. Symp., Montpellier, France (1996).

Manuscript received Oct. 10, 1995, and revision received Sept. 9, 1996.